processes

MDPI

Article

The Effect of pH Solution in the Sol–Gel Process on the Structure and Properties of Thin SnO_2 Films

Danatbek Murzalinov *,†, Elena Dmitriyeva †, Igor Lebedev, Ekaterina A. Bondar †, Anastasiya I. Fedosimova † and Ainagul Kemelbekova †

Institute of Physics and Technology, Satbayev University, Almaty 050013, Kazakhstan; e.dmitriyeva@satbayev.university (E.D.); i.lebedev@satbayev.university (I.L.); e.grushevskaiya@satbayev.university (E.A.B.); a.fedosimova@satbayev.university (A.I.F.); a.kemelbekova@satbayev.university (A.K.)

* Correspondence: d.murzalinov@satbayev.university; Tel.: +7-727-386-5536

† These authors contributed equally to this work.

Abstract: The synthesis of surface-active structures is important for creating many applications. The structural formation of SnO_2 thin films in the range from 1.4 to 1.53 pH is studied in this work. This process occurs on the surface of the sample in the range of 1.4 to 1.49 and in the volume in the range of 1.51 to 1.53. SnO_2 is formed after annealing at 400 °C, according to XRD. Doping NH_4OH to solution stimulates particle coagulation and gel formation. All of these have an impact on the transparency of samples investigated by spectrophotometric methods. By increasing the pH, the resistance raises at room temperature. The E_g calculation along the fundamental absorption edge shows that it is greater than 3.6 eV′ for SnO_2 films. According to the Burstein–Moss effect, a change of the bandgap is related to the increased concentration of the free charge carriers. Elemental analysis has shown that chlorine ions are considered to be additional sources of charge carriers. The value pH = 1.49 is critical since there is a drastic change in the structure of the samples, the decrease in transparency is replaced by its increase, and the energy of activation of impurity levels is changed.

Keywords: sol–gel; pH; thin films; tin oxide; transmission spectra; the activation energy of donor levels

Citation: Murzalinov, D.; Dmitriyeva, E.; Lebedev, I.; Bondar, E.A.; Fedosimova, A.I.; Kemelbekova, A. The Effect of pH Solution in the Sol–Gel Process on the Structure and Properties of Thin SnO_2 Films. *Processes* **2022**, *10*, 1116. https://doi.org/10.3390/pr10061116

Academic Editors: Spivak Yulia, Vrublevsky Igor and Haiying Tan

Received: 27 April 2022
Accepted: 25 May 2022
Published: 2 June 2022

1. Introduction

The sol–gel process combines a group of methods for materials synthesis from solutions, an essential element of which is a gel formation at one of the stages. The transformation of sols into gels is the basis of the latest nanotechnologies for the production of microbiological fuel cells, thin films, photocatalytic nanocomposite membranes, and other materials with unique properties and controlled structure [1–6].

Thin tin oxide films and composite systems based on them are used as active layers in gas analysis equipment. They are of great importance for the rapidly developing solar energy industry [7–11].

Pure, non-stoichiometric tin dioxide (SnO_{2-x}) is an n-type semiconductor with room-temperature conductivity. The presence of intrinsic defects—oxygen vacancies forming shallow donor levels—determines its conductivity. The formation energy of oxygen vacancies depends on the position of the Fermi level. When it is near the top of the valence band, the vacancy formation energy is negative, −0.3 eV, which leads to the spontaneous generation of defects [12,13]. Tin dioxide is transparent in the visible and near-ultraviolet regions. The combination of such optical and electrophysical properties determines a wide range of applications of this material. The properties of oxides significantly depend on synthesis technology and subsequent treatment [14]. Currently, several methods for producing tin dioxide films based on sol–gel technology are developed [15]. The most interesting are the hierarchical layers with controlled porosity. The addition of impurities into the initial solutions leads to the formation of a different

structure that determines the main properties of the films. In particular, the addition of nitrogen atoms in the SnO_2 nanostructure is used to improve gas sensitivity to acetone vapors.

The acidity level of the film-forming system solution is an important factor. The particle size, as well as the surface morphology of the film, depends on the pH. Moreover, this parameter significantly affects the rate of sol–gel reactions.

The work [16] shows that tin oxide nanoparticles were synthesized using the sol–gel method with pH change in the range from 6 to 12. The structural, morphological, optical, and electrophysical properties of the samples were studied depending on the annealing temperature. However, the films' properties were not considered with a change in pH less than the precipitation of tin acid. Dmitrieva et al. [17] draw attention to the change in pH upon the addition of NH_4F to the film-forming system. A comparison of the properties of SnO_2 films depending on pH is presented. However, there is no systematic approach to determining the effect of acidity on the structure and properties of films. Chen et al. [18] considered the synthesis of two-dimensional tin oxide structures using the hydrothermal method by adding $NH_3 \cdot H_2O$ (25% aqueous solution) to a solution in a volume of 3, 5, 7, and 10 mL, but the effect of the additive on the structure of the films was not taken into account. In the work [19], tin-doped indium oxide nanocrystals were prepared chemically at different pH values of solutions. A hydrophilic polymer, polyacrylic acid, was used in the synthesis. Homogeneous, smooth, and optically transparent thin films were deposited by spray coater. However, the effect of pH changes on the optical and structural properties of films without a polymer additive has not been studied yet. In the work [20], the deposition of tin oxide from thin hydrous tin tetrachloride was activated by the addition of ammonia (NH_4OH). Ammonia was added dropwise until the pH reached 12. The structural and morphological properties of SnO_2 were changed. At the same time, the research did not consider the change in acidity from the initial value to the pH of the precipitation of tin acid (pH $\approx$ 2). The novelty of the current observation comprises the consideration of the properties of SnO_2 films which are investigated when the pH changes are below the level of precipitation of tin acid by adding $NH_3 \cdot H_2O$ to the solution. The purpose of this research is to determine the pH range in which the changes of volumetric structure formation transfer to surface formation, and in this case the process of optical characteristics modifies, as well as surface resistance. An advantage of comprehensive study is the dependence of sample transparency and their resistance on the pH change of the film-forming system, which is very important for solar cells and sensors.

2. Methods

2.1. Materials and Synthesis

A crystalline tin tetrachloride hydrate ($SnCl_4 \cdot 5H_2O$) (pure) and rectified alcohol (GOST 5962-13) were used for the preparation of film-forming systems. The acidity of the film-forming systems was regulated by the addition of an aqueous solution of ammonia (high purity). Precleaned microscope slides with dimensions 76 × 26 × 1 mm were used as substrates for the film's deposition. The crystalline hydrate of the tin tetrachloride was crushed to a powdery state. A sample weighing 3.9072 g was placed in a 100 mL flask and dissolved in 50 mL of ethanol. Concentrated aqueous ammonia solution (0.2 mL; 0.4 mL; 0.8 mL; 1.2 mL; 1.6 mL; 2.0 mL; 2.4 mL) was diluted with ethanol to 25 mL and, dropwise, at constant stirring, was introduced into the initial solution. The resulting mixture was brought to 100 mL by adding ethanol to obtain a system with a tin ion concentration of 0.11 mol/L. In this case, the following reactions with ethanol occur in the $SnCl_4$/ethanol system:

$$SnCl_4 + xC_2H_5OH \rightarrow SnCl_{4-x}(C_2H_5O)_x + xHCl \quad (1)$$

The stability of alkoxy compounds of the general formula $SnCl_{4-x}(C_2H_5O)_x$ decreases as the number of chlorine atoms in the molecule decreases. Therefore, in solutions, they can only be in certain proportions [21]. Reactions with water also take place in the $SnCl_4$/ethanol system:

$$SnCl_4 + 4H_2O \rightarrow Sn(OH_4) + 4HCl \quad (2)$$

Interaction with water leads to the appearance of reactive OH groups and the subsequent processes of polycondensation and phase formation—a sol formation. Hydrochloric acid (HCl) released during reactions (1,2) suppresses hydrolysis and shifts the equilibrium of system (2) to the left. Complete hydrolysis and formation of tin hydroxide are unlikely under conditions of water shortage. Complete hydrolysis of tin tetrachloride occurs on the substrate surface under the influence of moisture from the air. The pH level was increased by adding an aqueous solution of ammonia, which has a slightly alkaline reaction due to the following process:

$$NH_3 + H_2O \rightarrow NH_4^+ + OH^- \quad (3)$$

Neutralization of HCl by adding an aqueous solution of ammonia occurs according to the following reaction:

$$NH_4OH + HCl \rightarrow NH_4Cl + H_2O \quad (4)$$

This catalyzes the hydrolysis of tin tetrachloride and the formation of tin hydroxide. The overall reaction is as follows:

$$SnCl_4 + 4NH_4OH \rightarrow Sn(OH)_4 + 4NH_4Cl \quad (5)$$

The film-forming systems were kept for a day in a dark place at 20 °C to establish a dynamic equilibrium between the substance molecules and the formation of stable chemical bonds. These conditions are necessary for the formation of a highly dispersed colloidal system (sol). The film deposition method. For deposition of thin films of SnO_2, we used the dip-coating method: The $SnCl_4$/ethanol system was deposited on the substrate (at an angle of 45°) by dipping into the solution and followed by drying at room temperature for 30 min. In this case, reactions (2,5) and the formation of tin hydroxide from alkoxy compounds occurred:

$$SnCl_2(C_2H_5O)_2 + 4H_2O \rightarrow Sn(OH)_4 + 2HCl + 2C_2H_5OH \quad (6)$$

In order to crystallize the structure, annealing was performed in a muffle furnace for 15 min at a temperature of 400 °C in an air atmosphere. The solvent (and other volatile compounds) evaporates and decomposition reaction of tin hydroxide into SnO_2 and water proceeds on the surface of the sample:

$$Sn(OH)_4 \xrightarrow{heating} SnO_2 + 2H_2O \quad (7)$$

To obtain a multilayer system, this process was repeated four times. Then the final annealing was carried out in a muffle furnace for 1 h at a temperature of 400 °C in an air atmosphere. The final thickness of the 4-layer film was about 166 ± 7 nm. The time interval between the deposition of individual layers was 1 h. As a result, 8 samples were obtained from film-forming systems with different pH.

2.2. Characterization Methods

The acidity of the systems was measured on a pH meter "pH-150M". The thickness of the layers was controlled by the micro-weighing method [22]. Four layers were deposited, with a thickness of about 166 ± 7 nm. The structure of the obtained SnO_2 films was studied using an analytical scanning electron microscope JSM-6490LA (JEOL). The transmission spectra were measured on an SF-256 UVI double-beam spectrophotometer (wavelength range 190–1200 nm). The DC resistance of the samples was determined using a UT58A instrument (UNI-Trend Technology Co., Ltd. (Guangdong, China)) in the range from 1 MΩ to 200 MΩ. The change in the resistance of the samples with increasing temperature was studied on an experimental setup that allows heating the substrate to 270 °C. The sample was mounted on a heating element and the resistance of films was determined between the clamping contacts, the distance between which was 8.5 mm. The XRD measurements were performed in the $\theta - 2\theta$ configuration using a DRON-6 system.

3. Results and Discussion

3.1. Influence of Chemical Parameters of Film-Forming Systems on the Structure of Films

Figure 1 shows the morphology of the sample surface, on which a film-forming system is applied without the addition of an aqueous ammonia solution (pH = 1.40). The flat surface of the sample can be seen in Figure 1a. At a magnification of 30,000 times (Figure 1b), sol particles are observed, formed during the maturation of the film-forming system. They have the shape of a unit cell SnO_2, shown in Figure 1c. The geometric parameters of the sol particles are 496.21 nm by 340.72 nm and their ratio is 1.46. This correlates well with the ratio of the unit cell parameters of tin oxide $a = 4.64A$, $c = 3.15A$, $a/c = 1.47$ [23]. Sol particles are fixed in a xerogel formed in accordance with the reactions (2,6,7).

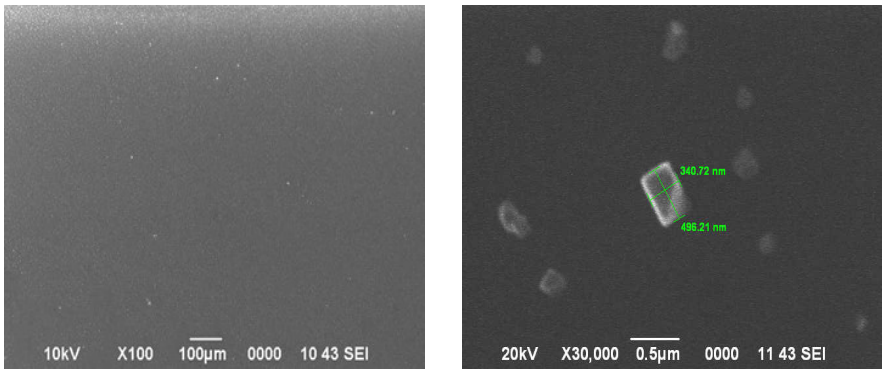

(**a**) (**b**)

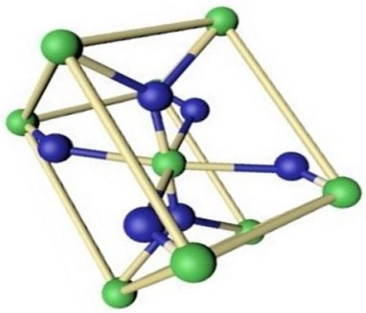

(**c**)

Figure 1. (**a**,**b**) The surface morphology of the sample surface, on which a film-forming system is applied without the addition of an aqueous ammonia solution. (**c**) Unit cell of SnO_2.

The fractal structures shown in Figure 2 begin to form in the film as the acidity increases to pH = 1.42. Their presence indicates nonlinear collective phenomena between particles [24]. The size of the formed clusters is up to 10 µm, the form of a six-petal flower (Figure 2b). The photograph taken at an angle of 80 degrees to the surface (Figure 2c) shows that the "petals" are formed by the raised sections of the film.

Figure 3 shows the surface morphology of films obtained from a film-forming system with pH = 1.44. It can be seen that the number of cluster structures has increased (Figure 3a), and their shape and size have also changed (Figure 3b). Along with flower-like structures (which in some cases increased to 50 µm), cruciform clusters appear. Figure 3b shows that the resulting clusters have a three-dimensional structure and rise above the total level of the layer surface.

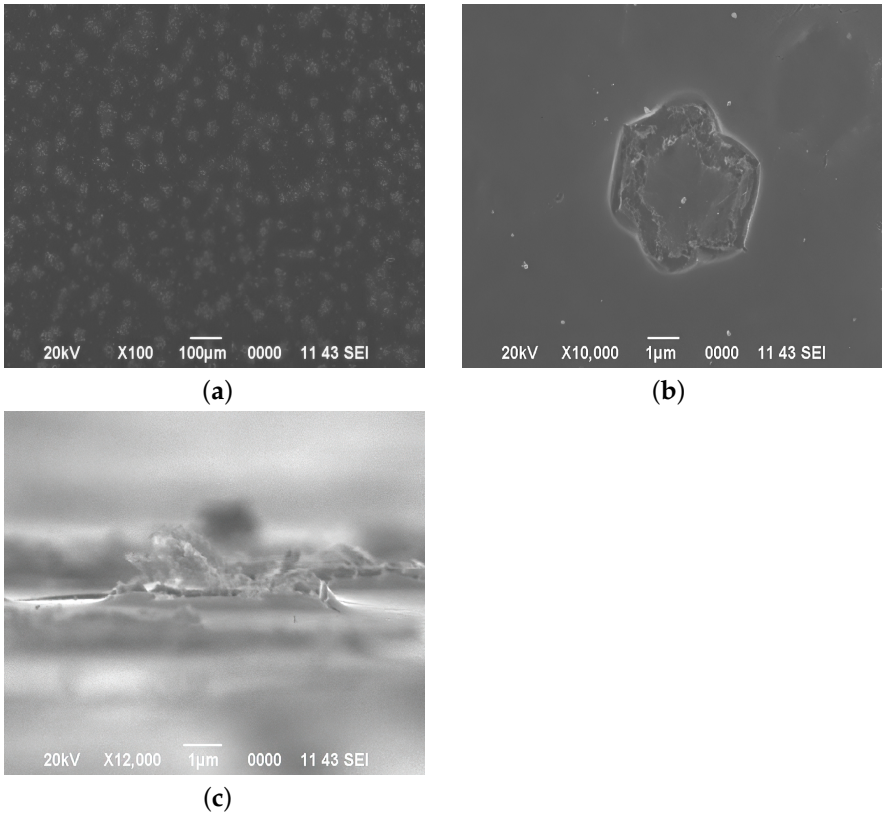

(**a**) (**b**)

(**c**)

Figure 2. The surface morphology of films deposited from a film-forming system with pH = 1.42. Top view: (**a**) ×100 magnification, (**b**) ×10,000 magnification, (**c**) profile view.

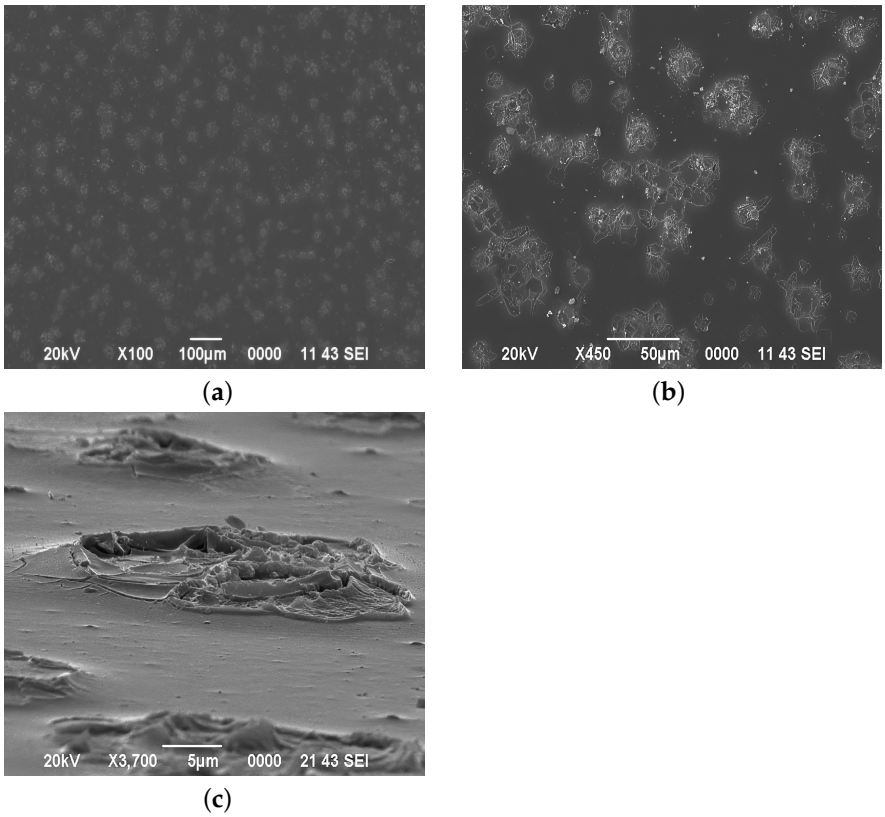

(**a**) (**b**)

(**c**)

Figure 3. The surface morphology of films deposited from a film-forming system with pH = 1.44. Top view: (**a**) ×100 magnification, (**b**) ×450 magnification, (**c**) profile view.

Dispersed particles do not precipitate in colloidal systems. In a suspended state, they are supported by a Brownian motion, but, unlike the usual Brownian motion of particles, dispersed particles in colloidal solutions cannot meet, which is due to the same charge of the particles of the dispersed phase. Gels are formed during coagulation (an adhesion of particles) of sols. To accelerate the coagulation process, catalysts are used that deform the electrical layer of the dispersed phase. The coagulation rate and the size of cluster structures depend on the catalyst concentration. The dominant mechanism for the formation of spatial structures is self-organization [25,26]. Along with the self-organization of particles formed in the film-forming system during maturation, the equilibrium in chemical reactions (5) shifts towards the formation of $Sn(OH)_4$ and NH_4Cl. In this case, the processes occur on the surface of the sample. Figure 4 shows the surface morphology of films deposited from a film-forming system with pH = 1.46.

Figure 4a shows a sharp increase in cruciform structures associated with an increase in pH to 1.46. In this case, the distribution of structures over the surface is irregular, which is associated with the multilayer nature of the films. The clusters formed during the deposition of the first layer are the points of growth of larger clusters in the second layer (Figure 4b). Along with this, self-organizing structures are formed between large clusters (Figure 4c). Figure 5 shows the surface morphology of films obtained from a film-forming system with pH = 1.47, pH = 1.49, pH = 1.51, and pH = 1.53.

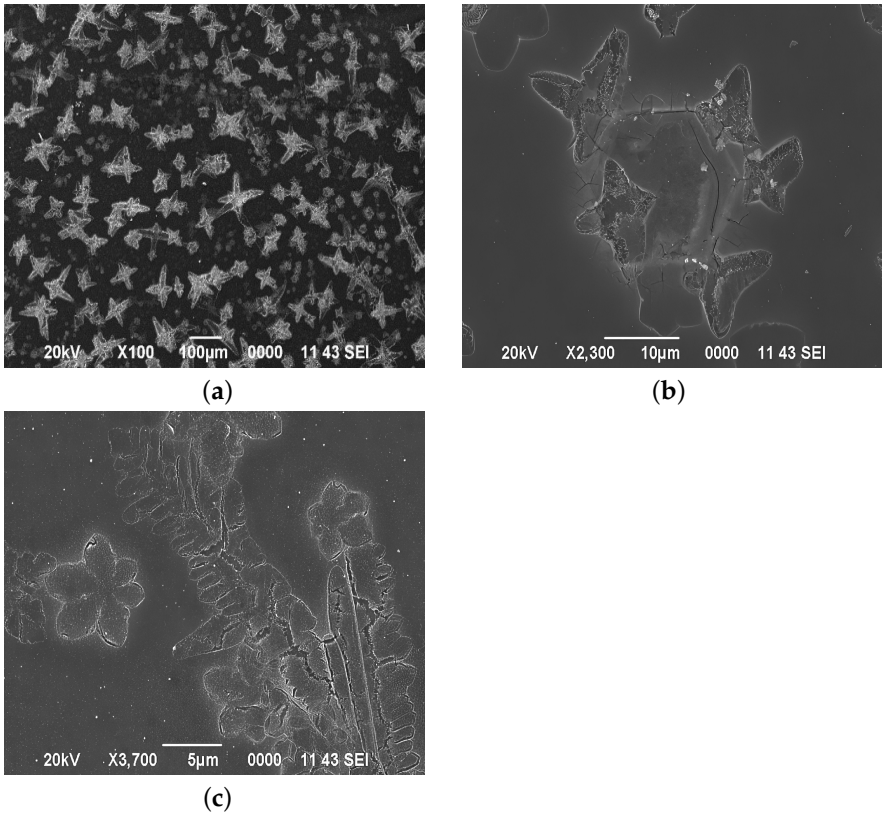

Figure 4. The surface morphology of films obtained from a film-forming system with pH = 1.46: (**a**) ×100 magnification, (**b**) the morphology of large clusters, (**c**) the morphology of the surface between large cluster structures (the area is marked with a red square).

A change in acidity to pH =1.47 leads to the formation of structures with the largest dimensions of 217.91 µm by 110.52 µm (Figure 5a). A further increase in pH leads to the formation of structures up to 442.40 µm in length. Under these conditions (pH = 1.49), the maximum number of cluster structures is observed on the sample surface (Figure 5b). An increase in the hydrogen index to pH = 1.51 and 1.53 leads to a decrease in the size of cluster structures, and their formation in the form of squares (Figure 5c). At pH = 1.53,

square clusters prevail, which is associated with the formation of NH_4Cl particles by reaction 5, which have a cubic unit cell (Figure 6).

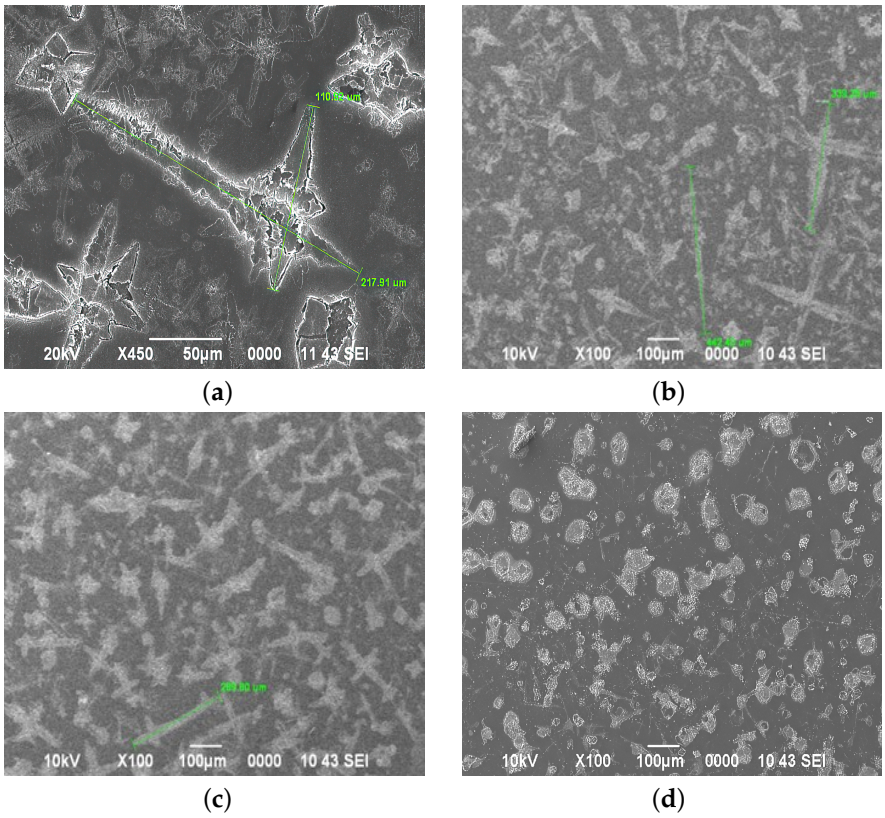

(**a**) (**b**) (**c**) (**d**)

Figure 5. The surface morphology of films deposited from a film-forming system with pH (**a**) 1.47, (**b**) 1.49, (**c**) 1.51, and (**d**) 1.53.

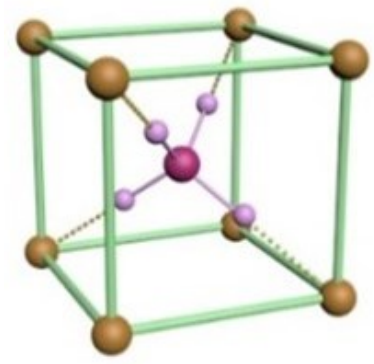

Figure 6. The schematic representation of the elementary unit cell of ammonium chloride.

The NH_4Cl particles formed in the bulk of the film-forming system are fixed in the gel-like structure of the film, similar to the SnO_2 particles shown in Figure 1. However, annealing the films at 400 °C, which is necessary for fixing the layer and the transition of the gel-like structure of $Sn(OH)_4$ into the SnO_2 xerogel, decomposes the cubic modification of NH_4Cl into volatile compounds according to the reaction:

$$N_4HCl \xrightarrow{T>337^\circ C} NH_3 + HCl \quad (8)$$

The transition from the solid to the gaseous state is accompanied by a sharp increase in volume, which leads to the partial destruction of the film. The pH of the formation of tin hydroxide ($Sn(OH)_4$) is 2. As the pH of the film-forming system approaches 2, the rate of

nucleation also increases. In the case of pH higher than 1.49, nuclei begin to form already in the bulk of the solution, and not on the surface of the substrate. The formation of tin hydroxide during the deposition of the film-forming system leads to the formation of separate large structures. In the case of pH = 1.40, the formation of tin hydroxide occurs in a thin layer of the film-forming system on the surface of the glass substrate. This is due to the evaporation of a part of the solvent and the formation of HCl during the reaction (2), upon interaction with H_2O from the air. Crystallization stops at the stage of nucleation.

3.2. Study of the Structure of Films

Figure 7 shows the X-ray diffraction on the crystal lattice of the sample with addition of 0.8 mL ammonium hydroxide per 100 mL of solution. In the XRD, against the background of a rather high noise level at the $2\theta = 32.92^{\circ}$, a clear signal is observed from the crystallographic planes of a cubic NH_4Cl (space group Pm-3m (221), PDF card number-01-073-0365) corresponding to the orientation plane (110) [27].

In the pristine sample (with no additives), the XRD of which is shown in Figure 8, no signals are detected.

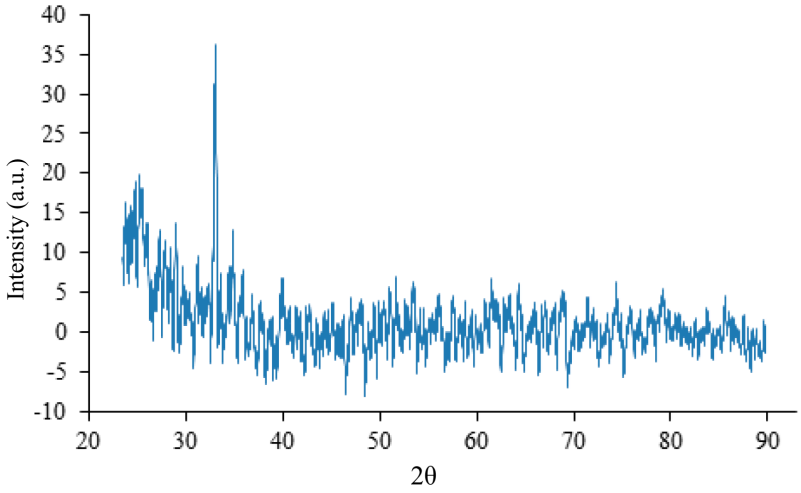

Figure 7. XRD of the sample with the addition of 0.8 mL NH_4Cl per 100 mL of solution with no annealing.

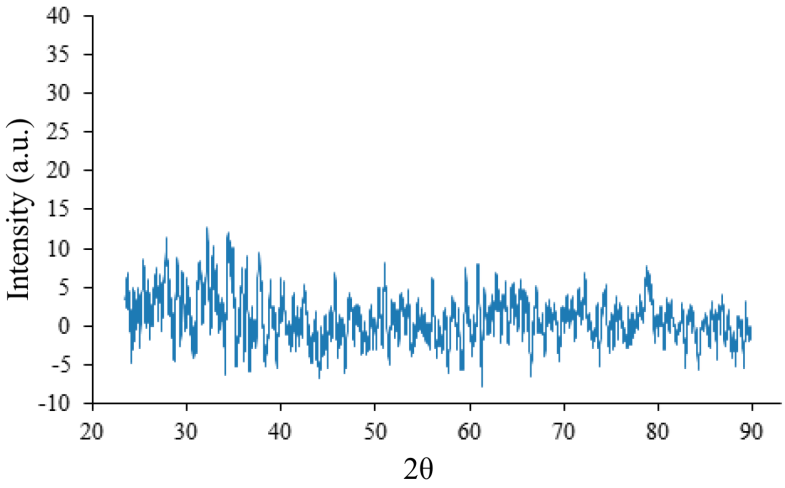

Figure 8. XRD of the sample with no annealing.

3.3. The Structure of the Films as a Function of the Annealing Temperature

Annealing of the prepared series of films was carried out at temperatures of 100 °C, 250 °C, 350 °C and 400 °C. In this case, with an increase in the annealing temperature, a significant increase in the signal amplitude is observed at angles $2\theta = 32.92°$ up to 350 °C. This is due to an increase in the concentration of ammonium chloride crystals. The signal amplitude reaches its maximum value and becomes four times higher at a temperature of 350 °C (Figure 9), compared to the spectrum of the sample shown in Figure 7. In addition, weak signals appear from the crystallographic planes of tin dioxide SnO_2—the hydrated form turns into a crystalline form.

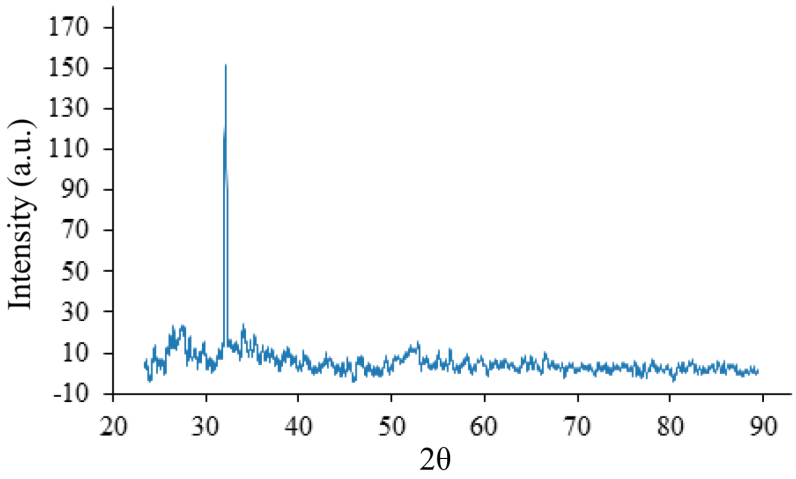

Figure 9. XRD on the crystal lattice of the initial sample, annealed at a temperature of 350 °C.

Four characteristic peaks of SnO_2 are distinguished at angles of $2\theta = 26.7°$, 33.9°, 38.1°, and 52.2° at annealing temperature 400 °C (Figure 10) in the XRD of the film. These signals correspond to the crystallographic (110), (101), (200), and (211) planes of a tetragonal SnO_2 (P42/mn(136) group, Powder Diffraction File (PDF) 88-0287) [28]. Signals from NH_4Cl are not detected. NH_4Cl is sublimated by decomposition into ammonia and hydrochloric acid.

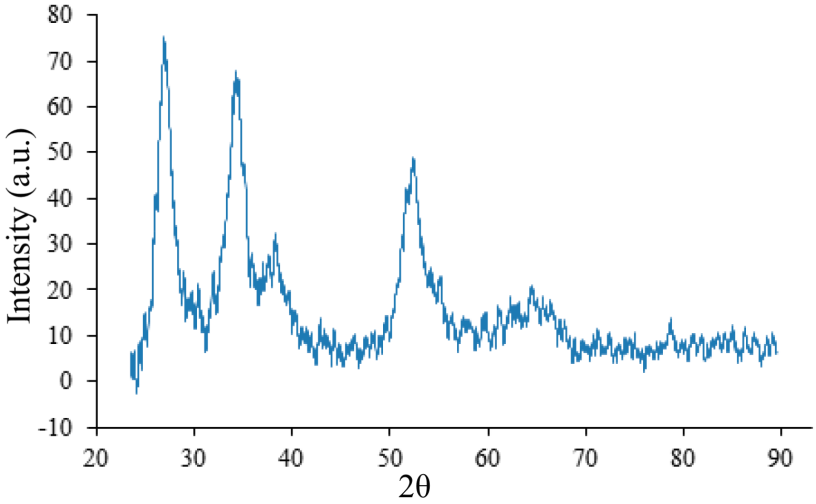

Figure 10. XRD on the crystal lattice of the initial sample, annealed at a temperature of 400 °C.

The counteraction of various direct and reverse chemical reactions of the sol–gel process along with coagulation and peptization in a dispersed medium at certain acidity against the background of diffusion leads to the establishment of a steady state with equilibrium concentrations.

3.4. Influence of the Chemical Parameters of Film-Forming Solutions on the Optical Properties of Films

Figure 11 shows the transmission spectra of thin films of tin oxide after the deposition of four layers of the solution; the concentration of tin ions is 0.11 mol/L, with the addition of various amounts of aqueous ammonia solution (0.2 mL; 0.4 mL; 0.8 mL; 1.2 mL; 1.6 mL; 2.0 mL; 2.4 mL). To compare the transparency of the obtained samples, the transmission spectrum of the glass substrate is presented (curve 1).

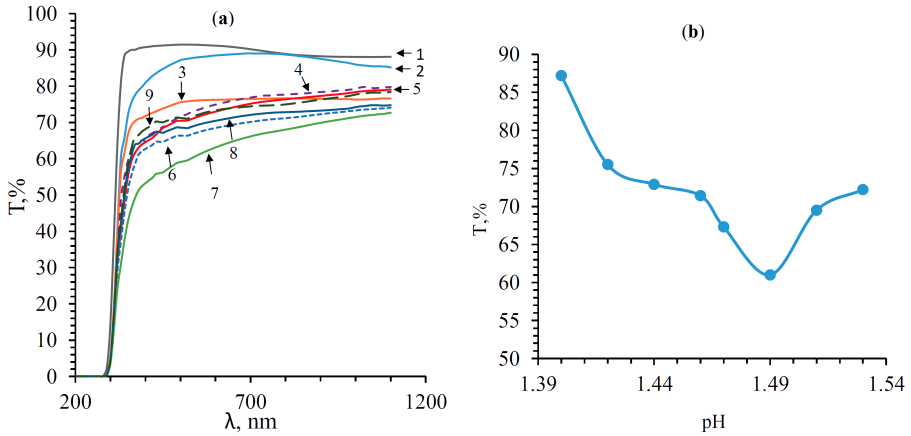

Figure 11. Transmission spectra of tin oxide thin films. (**a**) Transmission spectra: (1) the glass substrate; (2) pH = 1.40; (3) pH = 1.42; (4) pH = 1.44; (5) pH = 1.46; (6) pH = 1.47; (7) pH = 1.49; (8) pH = 1.51; (9) pH = 1.53. (**b**) Dependence of the transmittance in the visible range (400–700 nm) on pH.

Figure 11 shows that films with a film-forming system pH of 1.40 have a transparency of 85–90%. As the pH of the film-forming system increases, the transparency of films decreases. This is due to the scattering of electromagnetic radiation from surface irregularities. The transmission spectra of films obtained from the $SnCl_4$/EtOH system with pH = 1.51 and pH = 1.53 are higher than those with pH = 1.49, which correlates with the change in their surface morphology. Figure 11 shows the dependence of the transmittance on the pH level of the film-forming system of the studied films in the visible range (400–700 nm). It can be seen that the change in the transparency of the films with an increase in the pH of the film-forming system has a nonlinear form. A minimum of transparency is observed at pH = 1.49, corresponding to 61%. The bandgap was calculated from the fundamental absorption edge [29] from the transmission spectra, in the coordinates $(\alpha h\nu)^2$ versus $h\nu$. In this case, the extrapolation of the linear section to the $h\nu$ axis was carried out. The calculation results are shown in Figure 12. The bandgap of the glass substrate was E_g = 4.12 ± 0.005 eV (not shown in the graph). The results of bandgap calculations of the SnO_2 film are shown in Table 1. The optical bandgap of the SnO_2 films is greater than the fundamental E_g = 3.6 eV (Table 1) [30–32]. This broadening is explained by the Burstein–Moss effect [33]. At short wavelengths (high energies), interband transitions of electrons from the valence band to the conduction band limit the transmission. The partially filled conduction band, separated by an additional gap from the rest of the band, is formed due to the strong hybridization of Sn 5s states.

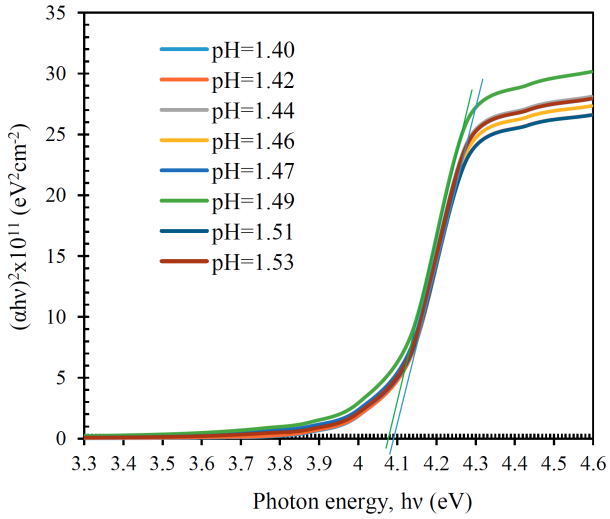

Figure 12. The $(\alpha h\nu)^2$ versus $h\nu$.

Table 1. Optical bandgap and Burstein–Moss shift.

Acidity of the Film-Forming System	Optical Bandgap, eV	$\triangle E_g^{BM}$, eV
1.40	4.09 ± 0.005	0.49 ± 0.005
1.42	4.09 ± 0.005	0.49 ± 0.005
1.44	4.09 ± 0.005	0.49 ± 0.005
1.46	4.09 ± 0.005	0.49 ± 0.005
1.47	4.09 ± 0.005	0.49 ± 0.005
1.49	4.08 ± 0.005	0.48 ± 0.005
1.51	4.09 ± 0.005	0.49 ± 0.005
1.53	4.09 ± 0.005	0.49 ± 0.005

The splitting of the conduction band promotes a decrease in optical adsorption due to transitions between its levels. A strong dispersion of the s-level of the conduction band, which is characteristic of most transparent conducting oxides, leads to a shift of the optical absorption edge towards higher energies with an increase in the concentration of charge carriers [34–37]. The filling of the dispersive conduction band leads to an increase in the energy required for the transition of an electron from the valence band to the conduction band (Figure 13).

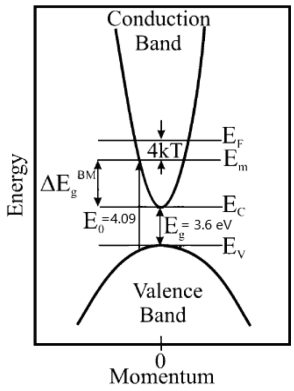

Figure 13. Diagram of the broadening of the optical bandgap due to the Burstein–Moss effect. E_g is the fundamental band gap and E_0 is the optical bandgap.

The broadening of the optical band gap by filling the conduction band ($\triangle E_g^{BM}$) is the difference between the optical bandgap (E_0) and the bandgap (E_g), as shown in Figure 13. The dependence of the charge concentration on the change in the optical band gap is expressed as follows [38]:

$$\triangle E_g^{BM} = \frac{h^2}{8m^*}\left(\frac{3}{\pi}\right)^{\frac{2}{3}} n^{\frac{2}{3}} \quad (9)$$

where h is Planck's constant, m^* is the effective mass of a carrier (electron) in the conduction band, and n is the number of charge carriers. The broadening of the optical bandgap increases the concentration of charge carriers. Consequently, the films contain excess (in addition to their own) free charge carriers. Their additional sources can be solvent ions and side results of reactions (H^+, Cl^-, OH^-, $C_2H_5^+$, NH_4). Figure 14 and Table 2 show the results of the elemental analysis.

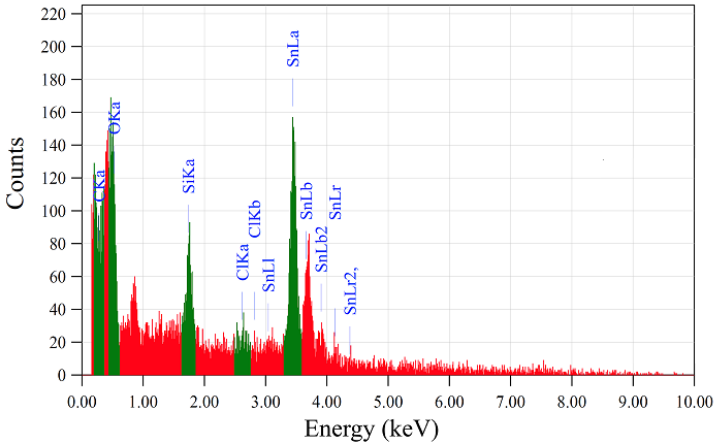

Figure 14. Elemental analysis of the film with no additives.

Table 2. Elemental analysis of the film.

Element	keV	Mass, %	Counts	Error, %
C	-	0	-	
O	0.525	3.97	352.09	0.03
Si	1.739	4.66	462.55	0.06
Cl	2.621	1.03	70.40	0.33
Sn	3.443	90.33	1585.18	0.02
Total	-	100	-	-

As can be seen from Figure 14 and Table 2, the presence of silicon atoms from the glass substrate, and the presence of tin, oxygen, and chlorine atoms are observed. Thus, it was found that chlorine ions are additional sources of charge carriers. Their presence in films in the form of impurities is confirmed by elemental analysis.

3.5. Investigation of the Electrophysical Properties of the Deposited Films

Thin films of tin dioxide SnO_2 belong to the group of non-stoichiometric semiconductors with an O/Sn ratio < 2. A change in the stoichiometric composition of SnO2 can be a consequence of an increase in the concentration of oxygen vacancies (SnO_{2-x}) or the presence of interstitial tin atoms ($Sn_1 + yO_2$) [39]. It was shown above that in addition to intrinsic charge carriers associated with a change in the stoichiometric composition, the conductivity of the films is due to the presence of impurity chlorine ions. To determine the activation energy of donor levels, the change in conductivity with increasing film

temperature was studied. The conductivity of semiconductors increases exponentially with increasing temperature according to the equation:

$$\triangle\sigma = \sigma_0 e^{-\frac{\triangle W}{2kT}} \quad (10)$$

where σ—conductivity, $\triangle W$—activation energy, k—Boltzmann constant, and T—temperature in Kelvin.

The dependence of natural logarithm of the conductivity on reciprocal temperature is shown in Figure 15. Two areas are observed under the acidity of the film-forming system pH = 1.40. The first is in the temperature range from room temperature to 160 °C ($1/T$ from 0.0034 K^{-1} to 0.0023 K^{-1}) with an activation energy of donor levels of 0.014 ± 0.001 eV. The second is in the temperature range above 160 °C with activation energy of donor levels of 0.697 ± 0.006 eV. Under the acidity of the film-forming system, pH = 1.42, in the temperature range from room temperature to 160 °C, two regions are observed with an activation energy of 0.014 ± 0.001 eV and 0.242 ± 0.002 eV. This is due to the formation of cluster structures in the film described earlier. Calculations of the activation energy of impurity levels for the rest of the samples are given in Table 3.

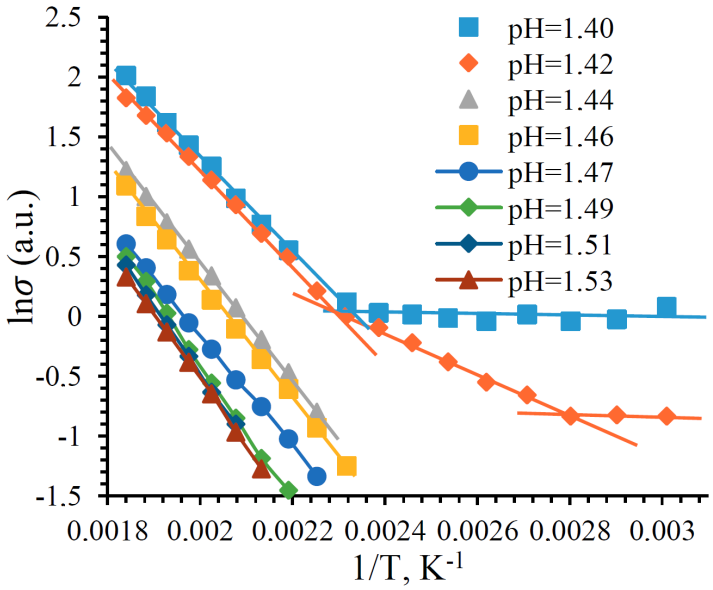

Figure 15. Natural logarithm of the conductivity versus inverse temperature.

Table 3. Optical bandgap and Burstein–Moss shift.

pH	*tgα*	$\triangle E \times 10^{-19}$, J	$\triangle E$, eV
1.4	4040 ± 33	1.1151 ± 0.0091	0.697 ± 0.006
1.42	4040 ± 33	1.1151 ± 0.0091	0.697 ± 0.006
1.44	4918 ± 57	1.3576 ± 0.0158	0.848 ± 0.010
1.46	4918 ± 57	1.3576 ± 0.0158	0.848 ± 0.010
1.47	4827 ± 57	1.3323 ± 0.0156	0.833 ± 0.010
1.49	5883 ± 70	1.6237 ± 0.0195	1.015 ± 0.012
1.51	5634 ± 64	1.5552 ± 0.0178	0.972 ± 0.011
1.53	5480 ± 61	1.5125 ± 0.0170	0.945 ± 0.010

Table 3 shows that the activation energy of the impurity levels increases with increasing pH to pH = 1.49, then it decreases. The relation between the pH of the film-forming system and the $\triangle E$ of films is connected to the formation of different film structures. The larger and more diverse the structural elements of the films, the greater the $\triangle E$, due to a decrease in the free path of the charge carriers.

4. Conclusions

The films deposited from a solution with a tin ion concentration of 0.11 mol/L without the addition of an aqueous solution of ammonia (pH = 1.40) have a relatively flat surface with inclusions of sol particles. The phase formation processes occur on the surface of the glass substrate after the evaporation of a part of the moisture from the $SnCl_4$/ethanol system. Water vapor from the air is involved in the hydrolysis of tin tetrachloride and the formation of tin hydroxide. The growth of surface structures, the correlation between which is stable, was found under increasing pH in the range from 1.4 to 1.49. Characteristic peaks of SnO_2 are distinguished in the XRD at annealing temperature 400 °C of the film. The transmittance of films is reduced to a minimum at pH = 1.49. With a further change of acidity in the range from 1.51 to 1.53, the square-shaped clusters prevail. This is due to the formation of NH4Cl particles in the volume of the film-forming system, which decompose when heated above 337.6 °C. It has been proven that in the process of increasing the concentration of NH_4OH in the solution, the rate of coagulation of particles and the size of cluster structures rise. The transition from the surface formation of the structure to the bulk occurs at pH = 1.49. The bandgap of the samples is greater than the fundamental value, which is associated with an increase of the concentration of free charge carriers. Chlorine ions are additional sources of charge carriers. The activation energy of the impurity levels rises under increasing pH to 1.49, then it decreases. It is related to the change in the free path of the charge carriers.

Author Contributions: Conceptualization, E.D. and I.L.; methodology, E.D.; software, A.K.; validation, E.D., I.L. and D.M.; formal analysis, A.I.F. and A.K.; investigation, D.M.; resources, E.D. and E.A.B.; data curation, A.K.; writing—original draft preparation, E.D.; writing—review and editing, I.L. and D.M.; visualization, A.I.F. and E.A.B.; supervision, D.M.; project administration, D.M.; funding acquisition, I.L. All authors have read and agreed to the published version of the manuscript.

Funding: This research was funded the program № AP09058002 «Investigation of the properties of dynamic memory based on Si3N4/Si and the formation of silicon nanoclusters with increased photoluminescence intensity» by the Committee of Science of the Ministry of Education and Science of the Republic of Kazakhstan.

Institutional Review Board Statement: Not applicable.

Informed Consent Statement: Not applicable.

Data Availability Statement: Not applicable.

Conflicts of Interest: The authors declare no conflict of interest.

References

1. Masalovich, M.; Ivanova, A.; Zagrebelnyy, O.; Nikolaev, A.; Galushko, A.; Baranchikov, A.; Loginov, V.; Shilova, O.; Kruchinina, I. Fabrication of composite electrodes based on cobalt (II) hydroxide for microbiological fuel cells. *J. Sol–gel Sci. Technol.* **2019**, *92*, 506–514. [CrossRef]
2. Ganbavle, V.V.; Kalekar, A.S.; Harale, N.S.; Patil, S.S.; Dhere, S.L. Rapid synthesis of ambient pressure dried tetraethoxysilane based silica aerogels. *J. Sol–gel Sci. Technol.* **2021**, *97*, 5–10. [CrossRef]
3. Gubanova, N.N.; Matveev, V.A.; Shilova, O.A. Bimetallic Pt/Pd nanoparticles in sol–gel-derived silica films and xerogels. *J. Sol–Gel Sci. Technol.* **2019**, *92*, 367–375. [CrossRef]
4. Shilova, O.A.; Gubanova, N.N.; Matveev, V.A.; Ivanova, A.G.; Arsentiev, M.Y.; Pugachev, K.E.; Ivankova, E.M.; Kruchinina, I.Y. Processes of film-formation and crystallization in catalytically active "spin-on glass" silica films containing *Pt* and *Pd* nanoparticles. *J. Mol. Liq.* **2019**, *288*, 110996. [CrossRef]
5. Lodh, S.; Ghosh, R.; Chakraborty, R. Studies on high refractive index amorphous TiO_2 thin film for possible improvement of light extraction efficiency in organic light emitting diodes. *Opt. Eng.* **2020**, *59*, 1107104. [CrossRef]
6. Yan, M.; Wu, Y.; Liu, X. Photocatalytic nanocomposite membranes for high-efficiency degradation of tetracycline under visible light: An imitated core-shell Au-TiO_2-based design. *J. Alloys Compd.* **2021**, *855*, 157548. [CrossRef]
7. Gordillo, M.A.; Panda, D.K.; Saha, S. Efficient MOF-Sensitized Solar Cells Featuring Solvothermally Grown [100]-Oriented Pillared Porphyrin Framework-11 Films on ZnO/FTO Surfaces. *ACS Appl. Mater. Interfaces* **2019**, *11*, 3196–3206. [CrossRef] [PubMed]

8. Ren, S.Q.; Li, H.Y.; Lei, C.; Li, C.Q.; Yin, X.H.; Wu, L.L.; Li, W.; Zhang, J.Q.; Wang, W.W.; Feng, L.H. Interface modification to enhance electron extraction by deposition of a ZnMgO buffer on SnO_2-coated FTO in CdTe solar cells. *Sol. Energy* **2019**, *177*, 545–552. [CrossRef]
9. Hossain, M.S.; Rahman, K.S.; Islam, M.A.; Akhtaruzzaman, M.; Misran, H.; Alghoul, M.A.; Amin, N. Growth optimization of ZnxCd1-xS films on ITO and FTO coated glass for alternative buffer application in CdTe thin film solar cells. *Opt. Mater.* **2018**, *86*, 270–277. [CrossRef]
10. Cirocka, A.; Zarzeczanska, D.; Wcislo, A.; Ryl, J.; Bogdanowicz, R.; Finke, B.; Ossowski, T. Tuning of the electrochemical properties of transparent fluorine-doped tin oxide electrodes by microwave pulsed-plasma polymerized allylamine. *Electrochim. Acta* **2019**, *313*, 432–440. [CrossRef]
11. Dong, Y.; Komarneni, S.; Wang, N.; Hu, W.C.; Huang, W.Y. An in situ anion exchange induced high-performance oxygen evolution reaction catalyst for the pH-near-neutral potassium borate electrolyte. *J. Mater. Chem. A* **2019**, *7*, 6995–7005. [CrossRef]
12. Kiliç, C.; Zunger, A. Origins of coexistence of conductivity and transparency in SnO_2. *Phys. Rev. Lett.* **2002**, *88*, 095501. [CrossRef] [PubMed]
13. Pronin, I.A.; Yakushova, N.D.; Karmanov, A.A.; Averin, I.A.; Moshnikov, V.A. Forms and concentration of adsorbed oxygen on the modified surface of SnO_2. *IOP Conf. Ser. J. Phys. Conf. Ser.* **2019**, *1313*, 012044. [CrossRef]
14. Nomura, K. Magnetic properties and oxygen defects of dilute metal doped tin oxide based semiconductor. *Croat. Chem. Acta* **2015**, *88*, 579–590. [CrossRef]
15. Ponomareva, A.A.; Moshnikov, V.A.; Suchaneck, G. Mesoporous sol–gel deposited SiO_2-SnO_2 nanocomposite thin films. *IOP Conf. Ser. Mater. Sci. Eng.* **2012**, *30*, 012003. [CrossRef]
16. Subramaniam, M.P.; Arunachalam, G.; Kandasamy, R.; Veluswamy, P.; Hiroya, I. Effect of pH and annealing temperature on the properties of tin oxide nanoparticles prepared by sol–gel method. *J. Mater. Sci. Mater. Electron.* **2018**, *29*, 658–666. [CrossRef]
17. Dmitrieva, E.A.; Mukhamedshina, D.M.; Mit', K.A.; Beisenkhanov, N.B. The effect of NH4F and NH_4OH on the structure and physical properties of thin SnO_2 films synthesized by the sol–gel method. *Glass Phys. Chem.* **2014**, *40*, 31–36. [CrossRef]
18. Chen, H.; Wang, X.; Guan, L.; Chen, L.; Tao, J. Surface engineering of layered *SnO* micro-plates for impressive high supercapacitor performance. *Mater. Chem. Phys.* **2019**, *238*, 121889. [CrossRef]
19. Maho, A.; Cabezas, C.A.S.; Meyertons, K.A.; Reimnitz, L.C.; Sahu, S.; Helms, B.A.; Milliron, D.J. Aqueous Processing and Spray Deposition of Polymer-Wrapped Tin-Doped Indium Oxide Nanocrystals as Electrochromic Thin Films. *Chem. Mater.* **2020**, *32*, 8401–8411. [CrossRef]
20. Karthik, T.V.K.; Maldonado, A.; de la L. Olvera, M. Synthesis of Tin Oxide Powders by Homogeneous Precipitation. Structural and Morphological Characterization. In Proceedings of the 9th International Conference on Electrical Engineering, Computing Science and Automatic Control, Mexico City, Mexico, 26–28 September 2012.
21. Suikovskaya, N.V. *Chemical Methods for Producing Thin Transparent Films*; Lenizdat: St. Petersburg, Russia, 1971; p. 200.
22. Dmitriyeva, E.A.; Mukhamedshina, D.M.; Mit, K.A.; Lebedev, I.A.; Girina, I.I.; Fedosimova, A.I.; Grushevskya, E.A. Ammonia sensors on the base of gadolinium doped tin oxide thin films and its characterization: Effect of doping concentration. *News Natl. Acad. Sci. Repub. Kazakhstan (Ser. Geol. Tech. Sci.)* **2019**, *433*, 73–79. Available online: www.geolog-technical.kz/images/pdf/g20191/231-241.pdf (accessed on 27 April 2022). [CrossRef]
23. Maheswari, S.; Karunakaran, M.; Chandrasekar, L.B.; Kasirajan, K. Ammonia sensors on the base of gadolinium doped tin oxide thin films and its characterization: Effect of doping concentration. *Phys. B Condens. Matter* **2021**, *602*, 412477. [CrossRef]
24. Temiraliev, A.; Tompakova, N.; Fedosimova, A.; Dmitriyeva, E.; Lebedev, I.; Grushevskaya, E.; Mukashev B.; Serikkanov A. Birth and fusion in a sol–gel process with low diffusion. *Eurasian Phys. Tech. J.* **2020**, *17*, 132–137. [CrossRef]
25. Fedosimova, A.I.; Dmitrieva, E.A.; Lebedev, I.A; Temiraliev, A.T.; Temiraliev, T.; Abishev, M.E.; Baitimbetova, B.A.; Ryabikinand, Y.A.; Serikkanov, A.S. Modeling the process of formation of fractal structures in thin films. *IOP Conf. Ser. J. Phys. Conf. Ser.* **2018**, *1141*, 012004. [CrossRef]
26. Shilova, O.A. Fractals morphogenesis and triply periodic minimal surfaces in sol–gel-derived thin films. *J. Sol–Gel Sci. Technol.* **2020**, *95*, 599–608. [CrossRef]
27. Pajarito, B.B.; Llorens, C.; Tsuzuki, T. Effects of ammonium chloride on the yield of carbon nanofiber aerogels derived from cellulose nanofibrils. *Cellulose* **2019**, *26*, 7727–7740. [CrossRef]
28. Lee, S.G.; Han, S.B.; Lee, W.J.; Park, K.W. Effect of Sb-Doped SnO_2 Nanostructures on Electrocatalytic Performance of a *Pt* Catalyst for Methanol Oxidation Reaction. *Catalysts* **2020**, *10*, 866. [CrossRef]
29. Fernandes, P.A.; Shongalova, A.; da Cunha, A.F.; Teixeira, J.P.; Leitao, J.P.; Cunha, J.M.V.; Bose, S.; Salome, P.M.P.; Correia, M.R. Phase selective growth of $Cu_{12}Sb_4S_{13}$ and Cu_3SbS_4 thin films by chalcogenization of simultaneous sputtered metal precursors. *J. Alloys Compd.* **2019**, *797*, 1359–1366. [CrossRef]
30. Mukhamedshina, D.M.; Mit', K.A.; Beisenkhanov, N.B.; Dmitriyeva, E.A.; Valitova, I.V. Influence of plasma treatments on the microstructure and electrophysical properties of SnO_x thin films synthesized by magnetron sputtering and sol–gel technique. *J. Mater. Sci.-Mater. Electron.* **2008**, *19*, S382–S387. [CrossRef]
31. Mukhamedshina, D.M.; Beisenkhanov, N.B.; Mit, K.A.; Dmitrieva, E.A.; Medetov, N.A. Application of thermal and plasma treatments for modification of SnO_2 thin films properties. *Perspekt. Mater.* **2012**, *1*, 35–42.

32. Vilca-Huayhua, C.A.; Paz-Corrales, K.J.; Aragon, F.F.H.; Mathpal, M.C.; Villegas-Lelovsky, L.; Coaquira, J.A.H.; Pacheco-Salazar, D.G. Growth and vacuum post-annealing effect on the structural, electrical and optical properties of Sn-doped In_2O_3 thin films. *Thin Solid Films* **2020**, *709*, 138207. [CrossRef]
33. Batzill, M.; Diebold, U. The surface and materials science of tin oxide. *Prog. Surf. Sci.* **2005**, *79*, 47–154. [CrossRef]
34. Baron, E.; Feneberg, M.; Goldhahn, R.; Deppe, M.; Tacken, F.; As, D.J. Optical evidence of many-body effects in the zincblende $AlxGa1-xN$ alloy system. *J. Phys. D Appl. Phys.* **2021**, *54*, 025101. [CrossRef]
35. Zhu, G.Y.; Fang, M.; He, S.Q.; Qin, F.F.; Yang, X.L.; Wang, Y.J.; Xu, C.X. Floating GaN whispering gallery mode micro-ring lasing with Burstein-Moss effect. *AIP Adv.* **2020**, *10*, 105023. [CrossRef]
36. Li, K.F.; Gao, Q.; Zhao, L.; Liu, Q.Z. Electrical and Optical Properties of Nb-doped $SrSnO_3$ Epitaxial Films Deposited by Pulsed Laser Deposition. *Nanoscale Res. Lett.* **2020**, *15*, 164. [CrossRef]
37. Liu, C.; Yuan, Y.; Zhang, X.; Su, J.; Song, X.; Ling, H.; Liao, Y.; Zhang, H.; Zheng, Y.; Ta, J.L. Doping Effect on Structural and Optical Properties of InTe Thin Films. *Nanomaterials* **2020**, *10*, 1887. [CrossRef] [PubMed]
38. Ch, L.; Fa, W.; He, J.; Ch, Y. Effects of different annealing temperatures on the physical, optical, and electrical characteristics and chemical bonds of Ga and FCo-doped ZnO films. *J. Mater. Res. Technol.* **2020**, *9*, 6331–6342. [CrossRef]
39. Kwoka, M.; Lyson-Sypien, B.; Kulis, A.; Zappa, D.; Comini, E. Surface Properties of SnO_2 Nanowires Deposited on Si Substrate Covered by Au Catalyst Studies by XPS, TDS and SEM. *Nanomaterials* **2018**, *8*, 738. [CrossRef]